CM² MAGAZINE

第 13 期

南方科技大学海洋磁学中心主编

创刊词

海洋是生命的摇篮，是文明的纽带。地球上最早的生命诞生于海洋，海洋里的生命最终进化成了人类，人类的文化融合又通过海洋得以实现。人因海而兴。

人类对海洋的探索从未停止。从远古时代美丽的神话传说，到麦哲伦的全球航行，再到现代对大洋的科学钻探计划，海洋逐渐从人类敬畏崇拜幻想的精神寄托演变成可以开发利用与科学研究的客观存在。其中，上个世纪与太空探索同步发展的大洋科学钻探计划将人类对海洋的认知推向了崭新的纬度：深海（deep sea）与深时（deep time）。大洋钻探计划让人类知道，奔流不息的大海之下，埋藏的却是亿万年的地球历史。它们记录了地球板块的运动，从而使板块构造学说得到证实；它们记录了地球环境的演变，从而让古海洋学方兴未艾。

在探索海洋的悠久历史中，从大航海时代的导航，到大洋钻探计划中不可或缺的磁性地层学，磁学发挥了不可替代的作用。这不是偶然，因为从微观到宏观，磁性是最基本的物理属性之一，可以说，万物皆有磁性。基于课题组的学科背景和对海洋的理解，我们对海洋的探索以磁学为主要手段，海洋磁学中心因此而生。

海洋磁学中心，简称 CM^2，一为其全名“Centre for Marine Magnetism”的缩写，另者恰与爱因斯坦著名的质能方程 $E = MC^2$ 对称，借以表达我们对科学巨匠的敬仰和对科学的不懈追求。

然而科学从来不是单打独斗的产物。我们以磁学为研究海洋的主攻利器，但绝不仅限于磁学。凡与磁学相关的领域均是我们关注的重点。为了跟踪反映国内外地球科学特别是与磁学有关的地球科学领域的最新研究进展，海洋磁学中心特地主办 CM^2 Magazine，以期与各位地球科学工作者相互交流学习、合作共进！

“海洋孕育了生命，联通了世界，促进了发展”。 21 世纪是海洋科学的时代，由陆向海，让我们携手迈进中国海洋科学的黄金时代

目 录

2020

刘青松

快过年了，仪式感与日俱增，大多人都会预想着大年三十过后，生活会有本质的变化，至少是一个新起点。

这种感觉其实是对生命节奏感的一种具体表现。

没有节奏，没有韵律，就不会有生命。在几十亿年前，地月系统逐渐稳定后，月亮带来了夜晚和白昼，地球自转轴的倾斜带来了四季。尽管早期的日夜更替比现在快，一年的天数也由此多出来很多，毕竟有了节奏，从而也谱写了生命的韵律。于是，生命就逐渐习惯了各种节点，并在人类的文化体系里得到了升华。

2020 是一个不可多得的年份，这引入了对称美。我们地球上的生命大多采用对称方式，这种方式在 DNA 设计方面比较高效。由于对称，重心比较好设置，稳定性也增加了许多。所以，看到 2020 这种对称的数据，增加了人生稳重的感觉。

今年刚好又是我的本命年，朋友不好意思说透：“你今年 36？”那已经是一个遥远的年代了。打开电脑，在安静的办公室搜寻出我所谓的记忆。听着 Modern Talking、Sabrina 等上世纪 80 年代歌星的荷东舞曲，年轻的力量又注入身体。这些巨星，在电脑的屏幕上依旧青春靓丽。有时候心里稍有歉疚，从弱因果关系上，确实是我把这些年轻人顶到了老年，包括父母和亲朋，而且相关系数非常高。

我自然非常喜欢这种上世纪 80 年代的气氛，歌颂的无论是爱情、友情还是亲情，都是那么有活力，充满正能量。

关键是节奏感，心脏的跳动都会随之附和的节奏感！

2020，我们要努力把生活安排得有节奏，要有生命的脉搏跳动，要鲜活，要有力量。

生活有压力，我们要努力让生活感到压力！

对科研的一些想法

李园洁

当我发现自己不再追求一定要做出完美的结果，而是想着用合理的假设，恰当的方法，严密的逻辑得到能够自圆其说的结果的时候，我觉得应该踏入了科研的大门。

横在我眼前可见而不得入的高墙忽然消失，广袤无际的大森林等着我去探险。科研的目的是往大说是认识世界，改变世界，往小说是提高认知，改良技术。发现认知或技术的不足，发现问题为前进指出一个方向，以知识储备为装备向前开路。前进过程中，有时候会原地打转，可能是知识体系存在欠缺，及时弥补；可能是遇到问题不知道怎么解决，可以和别人讨论交流说不定就有灵感；可能是正在做琐碎的小事，其实是扫除障碍，不过看起来不明显；还有可能是走错方向，进入死胡同，要调整方向，重新出发。有时候会感到迷茫，觉得自己做的没有任何意义。你做的工作可能几百年、几千年甚至更长的时间之后才能体现它的价值，到投入生产可能还有很多环节很多路走，这就像给大海里倒一滴水，但是谁知道呢，也许你的文章给别人启发，产生新的 idea，星星之火可以燎原，虽然给人类认识世界改变世界贡献出一点水，但还是有用的。有时候会有一些成就感，当你忍受煎熬和痛苦解决了一个个小问题的时候，当你收获新的思考和想法的时候，这也许就是科研的乐趣所在了。

这些只是我的一点鄙见，在科研道路上再走远点，可能会有新的看法吧。

对科研的认识

陈艇

半夜二点多哄完时不时作妖的娃，看到老师要求写对科研的理解的消息。躺床上想了想，脑中闪过的是大学毕业回家的火车上跟一位同校的老师聊天时说的“既然读研了就肯定是要继续做科研的”。 一晃这已经是十年前的事情。那时对科研并不了解，只是一腔不明所以的热情。也许是因为年轻，见识太少，认为做科研安静、可以沉浸于自己的思考。也许也是因为自己知识储备不够，懂得太少，总感觉还有好多未知在等着自己。十年过去了，对科研也有了一些认识。

科研是对知识的敬畏。在知识的浩海里，我们每个人手头在研究的内容都是沧海一粟。问做这些微不足道的探索有什么意义，等同于问某个人类个体存在的意义。相对于人类社会，某个人是渺小的。但没有这些渺小的个体，又怎么会有缤纷的人类社会。同样，有了每个科研工作者的研究，人类的知识才会开花。所以啊，我想应该带着一颗敬畏的心做好手头的小科研。

科研是一场不断完善自我的修行。初以为做科研要求高智商，哪知这个领域要求高智商、高情商、多学科知识、多技术背景。所以，英语不好，补英语，知识面不宽补知识，口头表达欠缺，找机会多练习，技术不会继续找人请教。到自己有学生时，又得学习怎样成为一名好的导师，嗯，那又将是慢慢长路一条。在个人成长的道路上有科研为伴，也算是一幢幸事吧。

科研是对立统一的。你说繁杂的实验很枯燥，但也会有解决实验出现的问题时的喜悦，还有实验时同门相互帮助的感动。你说数据难以解释，但也有经过严密逻辑推理而找到答案的自我满足。你说野外工作很辛苦，累得睡梦中不自觉的呻吟；但是又怎么会忘记野外时风吹麦浪、海上日落的美景。你说文章改了不下几十遍，也不知道改了几年，等文章发出来都已经麻木，但又怎么会忽略每改一次对数据、对科学问题的新的理解。你说科学问题很难找，但是当经过自己的思考从众多文献中发现研究领域的缺陷，大家忽略的问题时，未来不就有了方向？

总体，我想科研即人生，痛并快乐着，并且都是向着未知出发。

前言

岩石磁学这门学问到底难不难？

亦难亦不难！

面前一架钢琴，七个音阶，八十八个键。初学者很快就能了解其音阶，弹奏出哆来咪发嗦拉西，进而可以弹奏一些简单的乐曲。可是，弹钢琴无止境，大部分人会半途而废，也只有少数人成为钢琴大师。

岩石磁学这门学问类似于弹钢琴。我们会涉及几十到上百种参数，理解其中每一种参数的物理含义并不难，但想要把它们组合起来，难度系数会大增。想要达到随心所欲地解释出各种参数组合的物理意义，更是需要多年的积累与训练。于是乎，很多人就会停留在初学者的阶段，满足于对几个参数的应用，比如磁化率、非粘滞剩磁等等，不愿意进阶。所以，岩石磁学的最难点在于解释多种参数组合，就如同弹奏贝多芬的名曲一样。

岩石磁学中的岩石（Rock）是一种泛指，而不是专指固体岩石，几乎包含我们所见的一切物质，比如宇宙中来的陨石、地球上各种岩石、各类土壤、沙漠中的沙子、河湖海底的沉积物、空气中的粉尘、工厂的各种污染物等等。我们可以形象地把岩石磁学看成是一条章鱼，伸出去八只爪子，向各个学科渗透。所以，学岩石磁学最大的好处就是可以和各种专业进行学科交叉，走到学科前沿。

岩石磁学中的磁学等同于物理专业中的磁学，其物理理论基础和所用仪器是一样的。当然二者也有区别，最大的区别在于岩石磁学涉及的磁性矿物都是自然界中的不规则矿物，其形状不规则，粒径分布不均一，晶格中含有杂质，大多是几种矿物的组合等等，非常复杂。而物理学所涉及的矿物大多是标准矿物。

实际上在最初构建基本模型的时候，岩石磁学肯定要以标准磁性矿物为基础。比如，著名的岩石磁学家 David Dunlop 据说就有四个神奇的磁铁矿样品，用它们的性质发表了一系列的岩石磁学理论文章。姜兆霞博士在读博士期间，利用实验室合成的含铝赤铁矿构建了复杂的赤铁矿磁学体系，做出了重要贡献，为此也获得了 2019 年基金委优秀青年基金资助。这些研究都属于把物理磁学标准矿物的思想应用于岩石磁学，进而解决自然介质的复杂机理问题。

学习岩石磁学的人有两类背景：物理出身和地质出身。岩石磁学的目的是要对自然介质中所含磁性矿物的种类、含量、磁畴状态（与颗粒大小和形状有关）、化学计量纯度、氧化程度等等进行精细刻画，然后把这些物理信息再转化为相关的地质学信息，从而构建相关的地质、气候以及环境过程。因此，这门学问就涉及物理学和地质学两大学科基础。

很多时候，地质学出身的人不愿意看数学物理公式，一看到奇怪的符号就头疼。而物理学出身的人对地质过程了解不多，又很难把磁学物理性质和具体的地质过程挂钩。所以，学习岩石磁学的第二个难点就是如何平衡物理磁学背景和地质专业知识，只有二者都兼顾，才能把岩石磁学的功效发挥到极致，否则都难免会有失偏颇。

也正是由于第二个难点，目前并没有特别有效的专业书籍同时满足物理学和地质学的要求。如果初学者一开始就读 Dunlop 和 Özdemir 夫妇 1997 年写的《Rock Magnetism》，我敢保证，很快他就会失去耐心。书中通篇的公式几乎是一道不可逾越的鸿沟。我估计为了改变这一现状，Evans 和 Heller 在 2003 年写了一本浅显的书《Environmental Magnetism》。这本书隐藏了复杂的物理公式，更多的是把物理参数应用到地质问题和环境问题。但是，这样做的隐患就是缺乏对各种参数复杂性的理解，对复杂地质和环境问题的处理就难以胜任。

因此，学习岩石磁学的第三个难点就是缺乏一本深入浅出，把物理公式和地质应用平衡好的一本专业教材。这使得大多数向学习岩石磁学的人无法下手。

学习岩石磁学这门学问需要一种螺旋式上升的方法。我们很难通过一次学习，通过阅读一遍书就能把其中各种复杂的逻辑关系彻底搞清楚，更不用说熟练地应用。学而时习之，一遍一遍地理解，一遍一遍地训练才能达到熟能生巧。很多人没有注意到这门学科的特点，浅尝即止，学后就忘成了常态。不但降低了学习效率，还严重打击了学习积极性，乃至于学习了几年后，仍只能理解磁化率的一般物理含义。实际上，磁化率很复杂，它和磁性矿物的种类、粒径、工作温度、频率、外场大小等等都相关。如果真正理解了磁化率的各种复杂性质，可以肯定地说，他基本上已经跨越了初学者这个阶段。

“不忘初心，牢记使命。”

我们学习岩石磁学的最终目的是要解决地质问题。自然界中所含的磁性矿物具有三大功能。第一种就是它们能够在地磁场中定向排列，从而记录古地磁信息。第二种就是它们作为一种特殊矿物，其生成、运移、保存与转化等过程都受控于地质过程。第三种功能就是磁性矿物含铁，而铁则是生物不可或缺的元素。因此，磁性矿物就和生物过程联系起来。从海洋中取来一根钻孔，我们就可以从上述三个方面来对其研究。

如果我们把自然介质中磁性矿物的性质给厘定错了，那就会相应地得出错误的地质模型，与真实的信息离题万里。所以，岩石磁学是基础，是确保得到正确地质模型的关键，很多古地磁和环境磁学问题最后归根结底都是岩石磁学问题。比如中国东部大陆架长序列沉积物定年一直以来就是个难点，这主要因为该地区水浅，环境变化剧烈。除了陆源带来的磁铁矿，还有后期在还原环境下形成的硫化物胶黄铁矿。磁铁矿携带原生的沉积剩磁，而后者则是一种后期干扰信息。刘建兴博士瞄准了胶黄铁矿这个关键矿物，用系统的岩石磁学方法找出这些含有胶黄铁矿的层位，进而分析这些层位的古地磁信息是否可靠。经过这样的处理，他

得出的磁性地层就非常合理，彻底改变了前人的年龄框架，为构建陆架区准确的磁性地层做出了贡献。

总的说来，岩石磁学并不是一门特别容易学的学问。但是只要持之以恒，多学好问，拓宽知识面，活学活用，肯定能掌握其中的奥妙。

这本《岩石磁学演绎》就充当引路先锋，我将尽力平衡物理磁学和地质学的知识体系，把公式压缩到最少，把应用推广到最宽。

大家一起在知识体系中畅游，体会做学问的艰辛与快乐！

第一章：能量是源头

世间万物最根本的源头在于能量，能量最小化是物质及其状态稳定存在的基础。

和磁性矿物最相关的是热能和磁能。

关于热能，我们最好理解，只要改变温度就能改变磁性矿物所含的热能。显然，温度越高，热能越大。我们常说一个人非常着急，坐立不安，就像热锅上的蚂蚁一样。对于磁性矿物也是这样，当温度升高时，其内部结构就会变得不稳定。

那么这里提及的磁性矿物结构到底是什么结构？

首先最好理解的就是磁性矿物的晶格结构。铁元素在自然介质中可以有两种存在方式，第一种是以独立的离子方式存在，比如 Fe^{2+}和 Fe^{3+}。在黏土矿物中就含有大量的铁离子。这些铁离子当然具有磁性，会对外场产生响应。只要我们加一个外磁场，这些铁离子就像小磁针一样向外场方向偏转，产生磁化。然而，当我们把外场去除掉的时候，这些铁离子的磁化方向又重新变混乱，从而其整体磁矩变为零，我们把这种磁学性质称之为“顺磁性（paramagnetic）。

在这里，我们引入了磁化的概念。对于同样一个外场，有的物质就容易被磁化，有的物质就不容易被磁化。为了比较这种性质，我们用磁化率来表示。磁化率是衡量一个物质被磁化容易程度的量。

对于顺磁物质，它的磁化率（χ）、磁化强度（M）和外磁场（H）之间的关系非常简单：

$$M = \chi H$$

这是一个简单的正比例函数，其中磁化率 χ 是一个常数。

如果我们把 M 和 H 的关系画成图像，就会发现这是一个过第一和第三象限的直线，且通过原点。

我们立即就发现一个问题，外场 H 越大，磁矩 M 就越大。那么 M 可以无限大下去吗？如果那样的话，就不存在一个饱和的状态，所谓饱和是指当 H 再增大时，M 不再变化。

目前全球古地磁实验室所能加的最大磁场一般不超过 2.5 特斯拉（T，磁场单位 T 和温度符号 T 在本书中会混用，但是一般不会产生歧义），最大不超过 10 T。有些磁学实验室（比如英国利物浦大学的古地磁实验室）就有能产生 7-8 T 的外加磁场装置。即使是 10 T 也不能使得顺磁物质饱和，但是随着外场再加

大，比如到几十 T 以上的时候，外加磁场会对原子外面的电子磁矩产生影响，从而影响其磁学性质。

顺磁物质最大的特点就是，当外场去除后，它不携带剩磁（Remanent Magnetization），所谓剩磁就是“剩下的磁性”。

除了单个的铁离子状态，众多铁离子还可以连接成阵，就像全真七子的“天罡北斗阵”一样，相互支撑，相互联系，其效率就会大为增加。

铁离子和铁离子之间要想连接在一起，还需要中间媒介（比如氧离子或者硫离子）。我们在初中时就已经学了基本的化学离子键概念。氧离子就像牛郎，一边牵着一个孩子（铁离子）。关键在于，根据泡利不相容原理，这两个相邻铁离子的磁矩必须成反向排列。一个向上，另一个必须向下。只有这样，两个磁矩之间的相互作用能才最小。

我们想象一下，铁离子和氧离子在空间中定向排列，先排一层氧离子，其两边再各排一层铁离子。在每一层中，铁离子的磁化方向一致。但是在相邻两层中，铁离子的磁化方向必然反向。

有了这种晶格结构，铁离子之间就有了相互作用，从而也就引入了磁能。

于是磁能和热能之间就开始展开较量。磁能的作用是使得铁离子的空间结构保持稳定，而热能的作用是使得铁离子变成热锅蚂蚁，其磁矩方向变得凌乱。总的说来，当逐渐加热时候，热能克服磁能，铁离子的空间点阵结构就会慢慢被破坏，从而磁性矿物的整体磁矩就会降低。

当温度升高到一个特定温度时，铁离子之间的点阵结构被彻底打乱，那么这个温度我们把它定义为居里温度（对铁磁性和亚铁磁性矿物来说是 T_C）（对反铁磁性矿物来说是尼尔温度 T_N）。

所以，居里温度其实就是指磁性矿物的晶体结构被打乱的温度。那么在居里温度之上，磁性矿物处于什么状态呢？

我们再回想一下顺磁性物质，其铁离子之间相互不干扰。在 T_C 之上，由于热能的作用，铁离子之间也不存在相互作用了，那么这种状态也是顺磁性。

一定记住，在 T_C 之上，磁性矿物处于顺磁性状态！

可见如果铁离子之间的相互作用越强，T_C 就会越高，反之就会越低。

那么如何才能降低一种磁性矿物的 T_C 呢？

从上面的论述我们可以得到暗示，那就是降低铁离子之间的相互作用能。其中一个非常有效的方法是在磁性矿物的晶格里掺杂没有磁性的离子，比如铝离子 Al^{3+}或者钛离子 Ti^{4+}。统计意义上讲，晶格中这些没磁性的离子含量越高，单位体积内的铁离子含量就少，其相互作用能整体就会偏低，从而 T_C 降低。

我们举个例子，比如磁铁矿的 T_C 为 578°，而当晶格中加入钛离子变为钛磁铁矿后，其 T_C 就会比 578°低。再比如赤铁矿的尼尔温度大约是 685°。当赤铁矿的晶格中掺入铝离子后，其尼尔温度要低于 685°。

如果我们发现一种矿物的特征温度是 550°，它可能是含钛磁铁矿，也可能是含铝赤铁矿。这种多解性是岩石磁学的难点所在。

有一种矿物比较特别，那就是磁赤铁矿。这种矿物的化学分子式和赤铁矿一模一样，都是 Fe_2O_3，但是他们的晶格结构完全不同。所以，在化学世界里，不要看到相同的分子式就认为是一种矿物，有时它们差距甚远，比如金刚石和石墨。

磁赤铁矿具有磁铁矿的结构，但是要把磁铁矿晶格中的二阶铁离子全都氧化成三价铁离子。为了电荷平衡，就需要在磁赤铁矿中产生很多空位（Vacancy）。这场情况下，这种空位当然会降低铁离子的含量，使 T_C 降低。但是，实际情况刚好相反，磁赤铁矿的居里温度反而会高于 578°。

这又是为什么？难道和之前描述的理论不符？

我们可以逆向思维。在含有空位的情况下，磁赤铁矿的 T_C 高于磁铁矿的 T_C。这说明前者晶格中铁离子的相互作用能更大。也就是说磁赤铁矿单位体积内的铁离子含量不降反升。能够达到这一效果，说明磁赤铁矿的晶格结构更紧凑，其晶格参数更小，就像压缩饼干一样，只不过没有后者压缩得那么厉害。

所以，如果发现一个矿物的局里温度是 610°，这可能是含铝赤铁矿，也可能是磁赤铁矿。

稍微熟悉岩石磁学的人会有另外一个问题，磁赤铁矿较为让人迷惑的地方在于，它受热不稳定。比如，在研究中国黄土高坡上的古土壤样品时，在 300°和 500°之间，磁性（比如磁化率）会在加热时大幅度降低，温度还没达到 578°之前就已经转化为更为稳定，且磁性很低的赤铁矿了。

如果谁能提出这个问题，说明对岩石磁学有了一定的了解，并在实践中有了初步应用。

为了回答上述问题，我们还需要了解磁赤铁矿的另外一个性质，大颗粒的磁赤铁矿比小颗粒的磁赤铁矿具有更高的热稳定性，也就是说大颗粒的磁赤铁矿可以经受住 600 多度的高温。

文献导读

1. 高精度 MIS 11 石笋记录类似于全新世以来亚洲夏季风变化

翻译人：仲义 zhongy@sustech.edu.cn

Xinnan Zhao, Hai Cheng, Ashish Sinha, et.al., ***A high-resolution speleothem record of Marine Isotope Stage 11 as a Natural Analog to Holocene Asian Summer Monsoon Variations [J],*** *2019,* ***Geophysical Research Letters****, 2019, 10.1029/2019GL083836.*

摘要：对过去间冰期内完整的谱分析是研究和探索现今间冰期气候变化的必要条件。我们采集了中国永兴洞石笋记录的氧同位素 11 期中的间冰阶（MIS11c）以来的亚洲夏季风信号。基于前所未有的年代限制和年代际尺度的时间分辨率为我们对 MIS 11c 和全新世之间的亚洲夏季风变化提供重要基础。我们的结果显示两次间冰期中轨道和百年尺度的运行速率和结构变化明显相似。值得注意的是，一个增强的千年尺度季风信号要晚于 MIS11c，被认为是“晚 MIS 11c 位移”，这个特征类似于亚洲夏季风的在晚全新世的增强特征，即“2 ka 位移”。如果只考虑自然营力的变化，在 MIS 11c 末期的百年尺度夏季风减弱可能意味着百年纪的夏季风减弱可能会持续到未来。

ABSTRACT: A full-spectrum characterization of past interglacial climate is a necessary prerequisite for the detection and attribution of climate changes during the current interglacial. Here we present a speleothem record of Asian summer monsoon (ASM) during Marine Isotope Stage (MIS) 11 interglacial (MIS 11c), from Yongxing cave, China. The record's unprecedented chronologic constraints and decadal-scale temporal resolution allow a precise and direct comparison of ASM between the MIS 11c and the Holocene. Our data suggest that orbital-centennial patterns of ASM were remarkably similar during both interglacial, including their pacing and structure. Notably, a multi-millennial stronger monsoon late in MIS 11c, the “Late-MIS 11c shift,” is similar to the Late Holocene strengthening of the ASM, the “2-Kyr shift.” Thus, the multicentennial ASM weakening at the end of the Late-MIS 11c shift could imply that the current century-long ASM waning trend may persist into the future, if only natural forcings are considered.

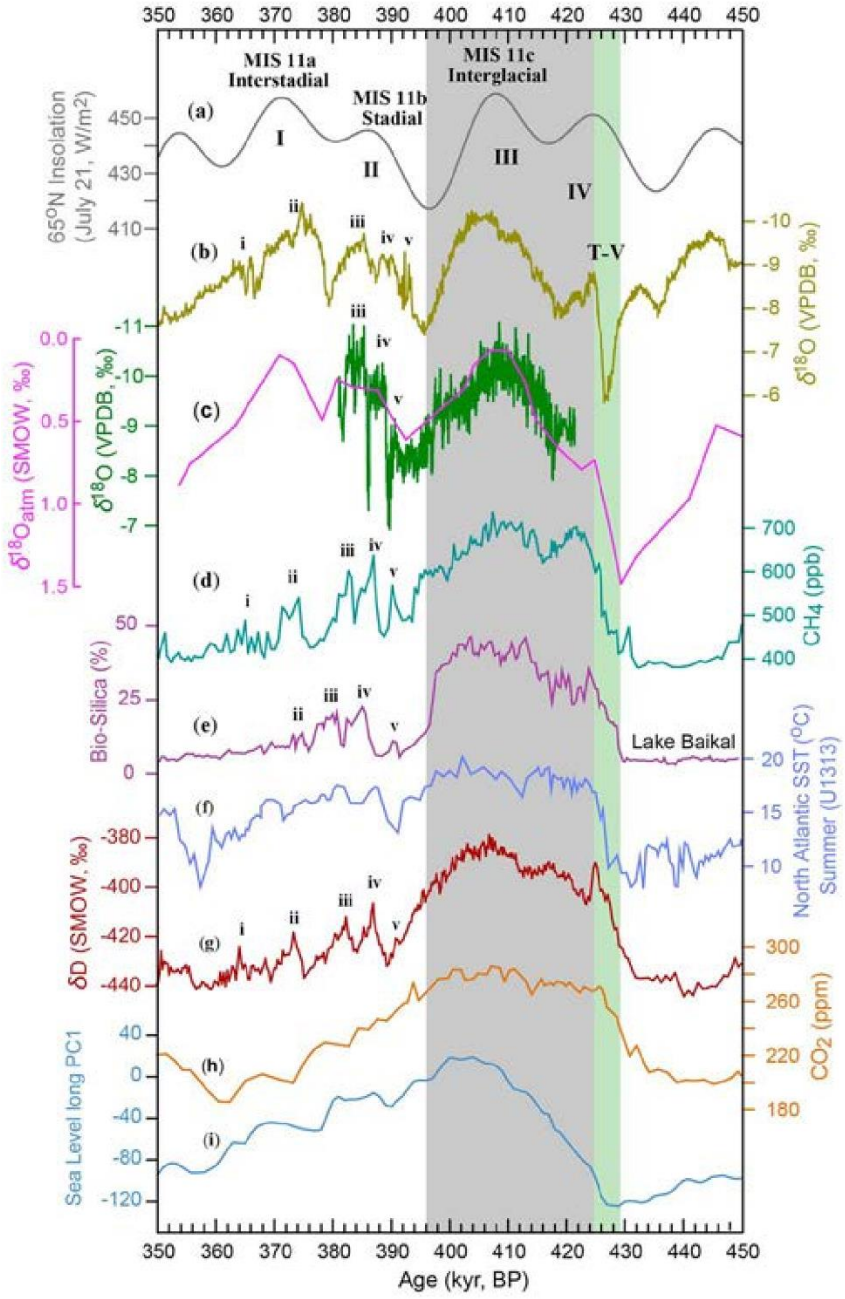

Figure 1. Holocene climate variations in the context of MIS 11. (a) The 21 July insolation at 65°N (Laskar et al., 2004). (b) Dongge record (Dykoski et al., 2005; Wang, 2005). (c) Yongxing record (this study). Red dash lines in (b) and (c) indicate the trends modeled by Ramp regression program (Mudelsee, 2000). Light blue bar in (b) and (c) indicate the temporal durations of the "2-Kyr shift" and "Late-MIS 11c shift," respectively. (d) to (g) Atmospheric CH4 (Loulergue et al., 2008), CO2 (Lüthi et al., 2008), Antarctic relative temperature (Jouzel et al., 2007), and sea level (inferred from benthic δ18O data; Spratt & Lisiecki, 2016), respectively. Gray and green curves depict the Holocene and MIS 11 records with their timescales at bottom and top, respectively. The climate conditions of the early Holocene and corresponding portion of MIS 11c are approximately similar (yellow bar). VPDB = Vienna Pee Dee Belemnite; MIS = Marine Isotope Stage.

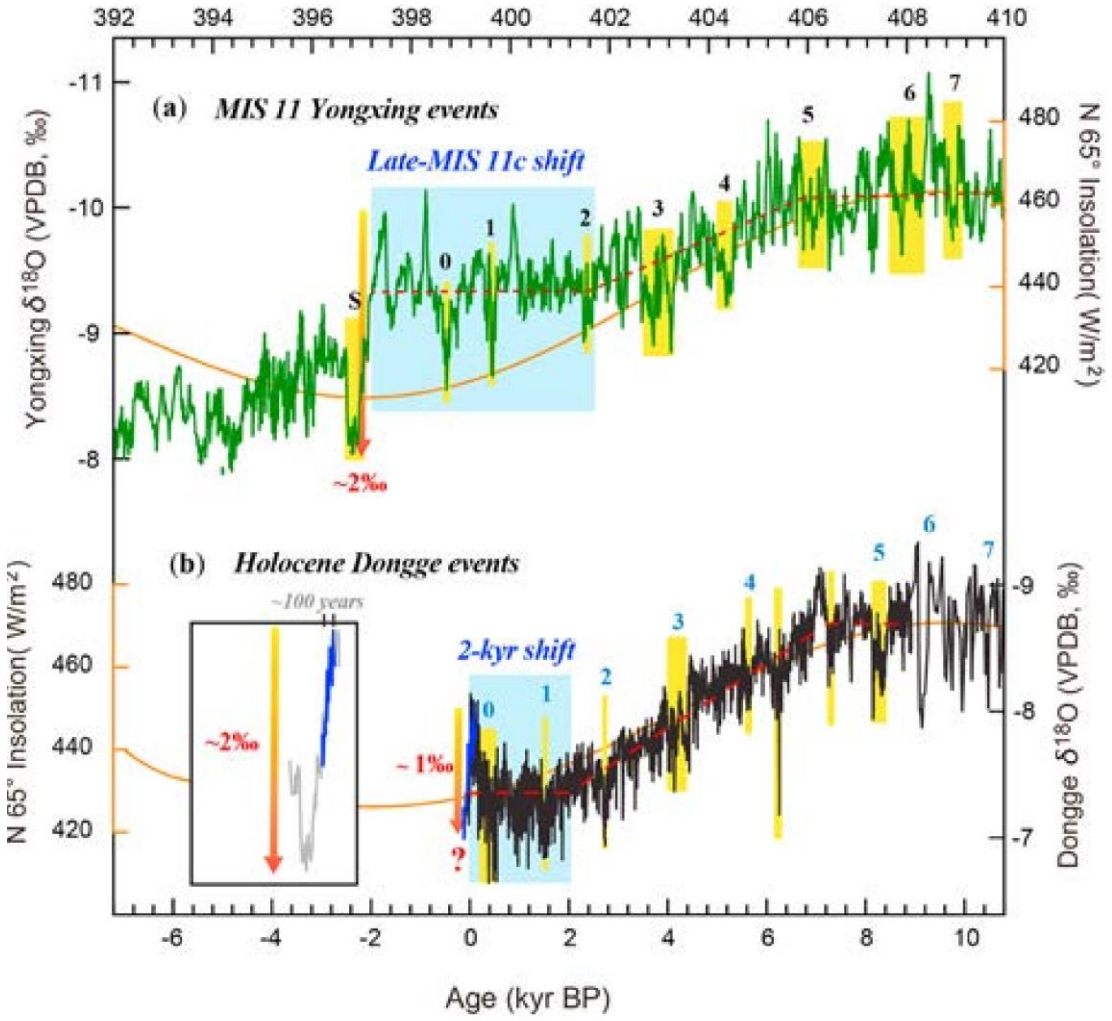

Figure 2. Comparison between ASM records during the Holocene and MIS 11c. (a) The Yongxing record (this study, green line) and 21 July insolation at 65°N (orange line; Laskar et al., 2004). Vertical yellow bars depict the Yongxing events (labeled by S and 0–7) during MIS 11c (Figure S9). Vertical arrows depict amplitudes (~2‰) of "Yongxing event S." The "Late-MIS 11c shift" in the late MIS 11c is shown by blue bar with a duration of ~4 Kyr. (b) Dongge record (Dykoski et al., 2005; Wang, 2005; black line) with 21 July insolation at 65°N (orange line; Laskar et al., 2004). Vertical yellow bars depict weak monsoon events possibly linked to Bond events (Wang, 2005). Vertical arrows depict amplitudes (~1‰) of last ~100-year trend of the ASM (Li et al., 2017; blue line). The 2-Kyr shift (Cheng et al., 2016) in the Late Holocene is shown by blue bar with a duration of ~2 Kyr. Blue curves in inset box show the last ~100-year trend of the ASM (Li et al., 2017) in comparison with an interval marking the abrupt culmination of the Late-MIS 11c shift (gray line, this study) at the end of MIS 11c. Vertical arrows (insert box) depict amplitudes (~2‰) of the Yongxing event S. Red dashed lines in (a) and (b) indicate the MIS 11c and Holocene trends revealed by the Ramp regressions (Mudelsee, 2000), respectively. The MIS 11c (Yongxing) and Holocene (Dongge) records are aligned via their insolation maxima at 408 and 9 Kyr BP, respectively. VPDB = Vienna Pee Dee Belemnite; ASM = Asian summer monsoon; MIS = Marine Isotope Stage.

2. 模拟多畴磁铁矿的磁化-使用扫描磁显微镜数据的多步参数反演

翻译人：柳加波

Pastore Z, Church N S, McEnroe S A. ***Multi-step parametric inversion of scanning magnetic microscopy data for modeling magnetization of multidomain magnetite[J]. Geochemistry, Geophysics, Geosystems****, 2019.*

摘要：地表岩石的总磁化强度取决于两个组分：基于地球外围磁场的感应组分；以及独立于当前地磁场的岩石剩磁组分。后者可以在地质历史时期保持长久的稳定，但岩石剩磁也易受到扰动导致复杂的磁历史记录。此外，样品的总磁化强度是所有具有保持磁化强度能力的磁性颗粒的贡献之和。现代磁学技术可以识别出不同粒径的贡献，并可用于评估磁化强度保持得如何，以及哪些地质事件可能影响了样品的磁稳定性。这样的解释需要根据强度和方向来估计离散颗粒的磁化强度。这些信息可以通过对岩石中磁性颗粒引起的磁场异常进行有限反演来获得。在这里，我们提出了一种工作流程，可将适用于薄片或厘米级岩心样品的磁力数据进行反演，并显示反演结果与矿物的实测体积性质和光学观察结果一致。

ABSTRACT: The total magnetization of a rock exposed at the Earth's surface is the result of two components: the induced component, which is dependent on the Earth's ambient magnetic field; and the magnetic memory retained in the rock, which is independent of the present Earth's field. The latter can be stable for long periods of geological time scales or be susceptible to changes resulting in complicated magnetic history record. Furthermore, the total magnetization of a sample is the sum of contributions of all the magnetic grains with varying abilities to retain a magnetization. Modern magnetic techniques allow the identification of contributions from the different grains and can be used to evaluate how well the magnetization is retained, and what geological events may have influenced samples' magnetic stability. Such interpretations require an estimation of discrete particle magnetization in terms of intensity and direction. This information can be achieved by constrained inversions of the magnetic field anomalies caused by the magnetic particles in the rock. Here, we present a workflow to invert magnetometric data applicable to thin sections or cm-sized core samples and show that inversion results are consistent with the measured bulk properties and optical observations of the minerals.

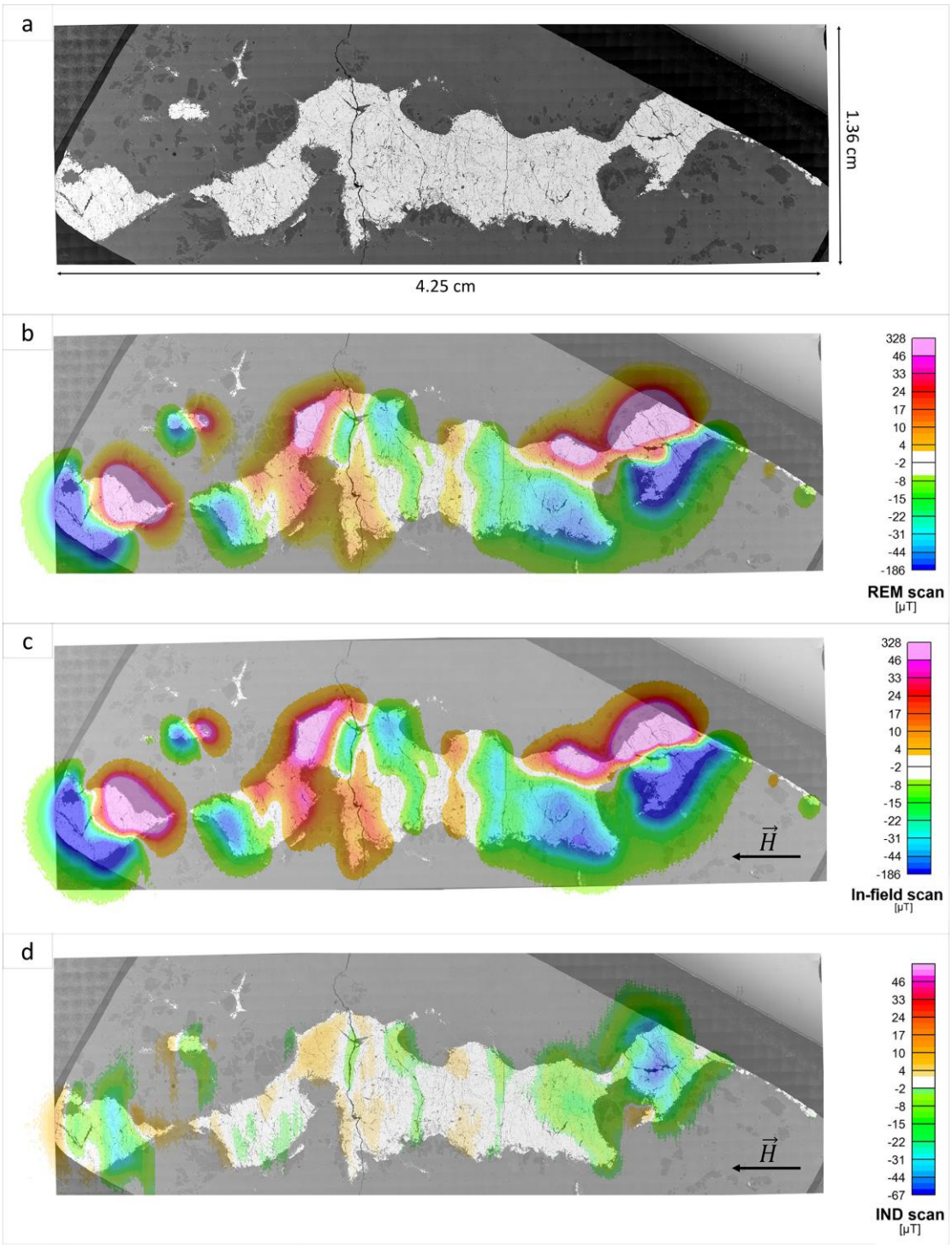

Figure 1. (a) Electron backscatter image of the sample. (b) An overlay of the REM-scan on the SEM image. (c) An overlay of the in-field scan on the SEM image, for a field $\vec{H}$ of 38 μT applied in the plane of the sample. (d) An overlay of the IND scan for a field $\vec{H}$ of 38 μT applied in the plane of the sample on the SEM image. The black arrows in (c) and (d) indicate the direction of the applied field.

3. 印度洋过去两千年气候驱动的海平面降低

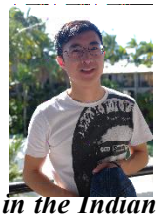

翻译人：蒋晓东 jiangxd@sustech.edu.cn

Kench, P. S., McLean, R. F., Owen, S. D. et al. ***Climate-forced sea-level lowstands in the Indian Ocean during the last two millennia****[J].* ***Nature Geoscience*** *(2019), 1-4.*

摘要：重建过去两千年的海平面变化，提供工业化前的背景信息用以评估现代海平面变化大小与速率是否是史无前例的。印度洋在过去两千年的海平面变化记录是非常稀缺的，而大西洋和太平洋的记录揭示海平面变化小于 0.25 米，并且无显著的负漂移。基于小环礁珊瑚化石的海平面记录，本研究发现在印度洋马尔代夫出现了两次低海平面事件。小环礁的生长受控于海平面，因此强有力的记录了过去的海平面变化。基于 U-Th 定年，马尔代夫珊瑚在公元 234-605 年与公元 1481-1807 年间出现了两次海平面低值，分别达到-0.88 米与-0.89 米。这两个低值同步于晚古小冰期和小冰期，具明显的太阳辐射减弱和海表面温度均降低。本研究提供了这两个小冰期时高保真的低海平面变化数据，其变化速率达到 4.24 毫米/年。研究结果进一步确认过去两个世纪加速的海平面相对上升，并且表明当前的海平面变化速率和大小并不是空前的。

ABSTRACT： Sea-level reconstructions over the past two millennia provide a pre-industrial context to assess whether the magnitude and rate of modern sea-level change is unprecedented. Sea-level records from the Indian Ocean over the past 2,000 years are sparse, while records from the Atlantic and Pacific Oceans show variations less than 0.25 m and no significant negative excursions. Here, we present evidence of two low sea-level phases in the Maldives, Indian Ocean, based on fossil coral microatolls. Microatoll growth is constrained by low water levels and, consequently, they are robust recorders of past sea level. U–Th dating of the Maldivian corals identified lowstands at ad 234–605 and ad 1481–1807 when sea level fell to maximum depths of -0.88 m and -0.89 m respectively. These lowstands are synchronous with reductions in radiative forcing and sea surface temperature associated with the Late Antiquity Little Ice Age and the Little Ice Age. Our results provide high-fidelity observations of lower sea levels during these cool periods and show rates of change of up to 4.24 mm yr-1. Our data also confirm the acceleration of relative sea-level rise over the past two centuries and suggest that the current magnitude and rate of sea-level rise is not unprecedented.

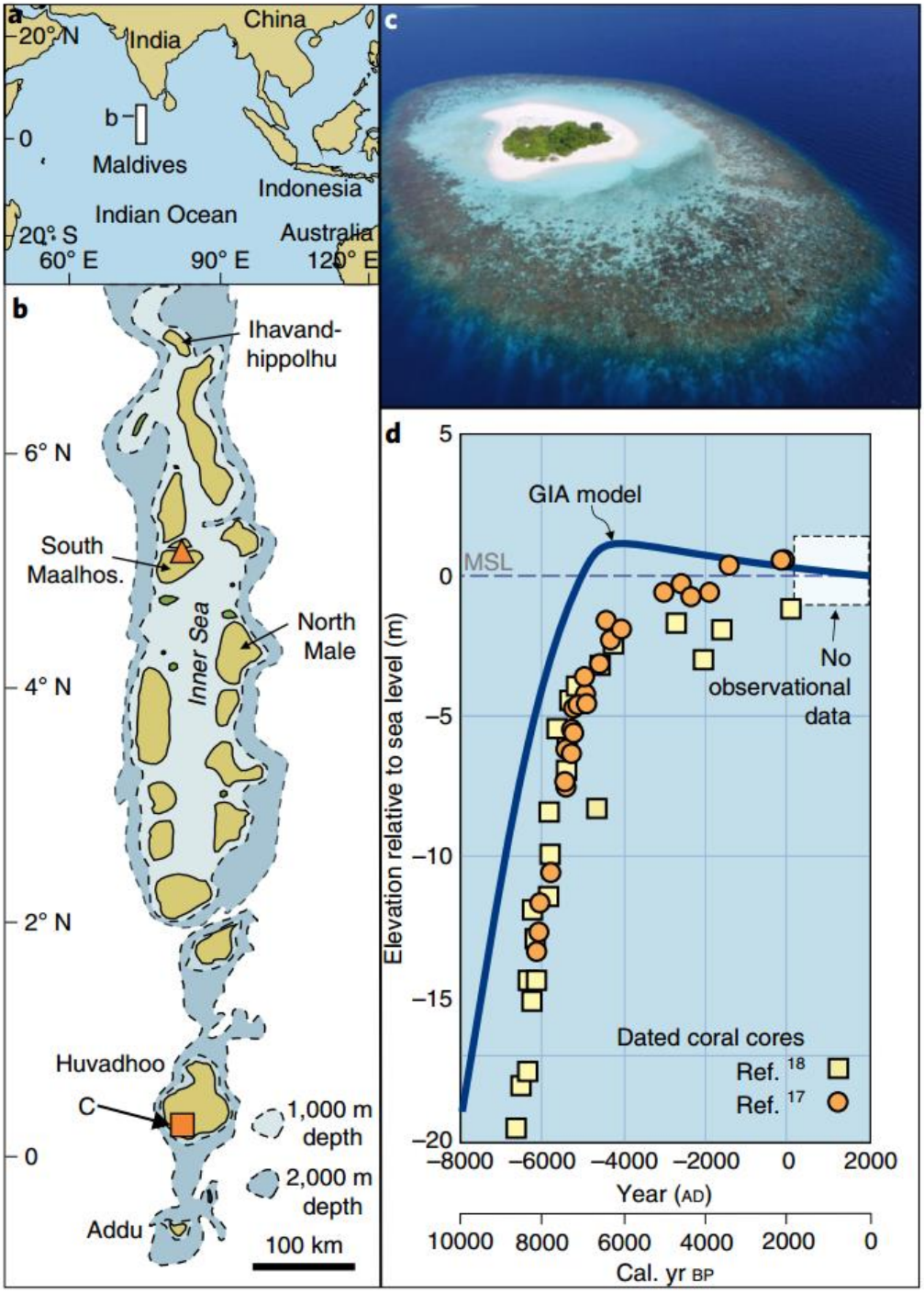

Figure 1. Field location and Holocene sea-level history of the Maldives archipelago, Indian Ocean. **a**, The location of Maldives archipelago, central Indian Ocean. **b**, The locality of the Mahutigalaa reef platform, Huvadhoo atoll (orange box), southern Maldives and the location of emergent mid-late Holocene corals in central Maldives (orange triangle). Base data British Admiralty Chart 709. **c**, An oblique aerial photograph of the Mahutigalaa reef platform (P.K., 2016). **d**, A summary Holocene sea-level curve for the Maldives based on published coral data and output from the GIA model ICE-6G_C (VM5a) for Mahutigalaa, see Methods for details. MSL, mean sea level; Cal. yr bp, calibrated years before 1950. No observational data indicates no physical coral evidence to support sea-level reconstructions, dated from the last 1,800 years, has been reported from the Maldives.

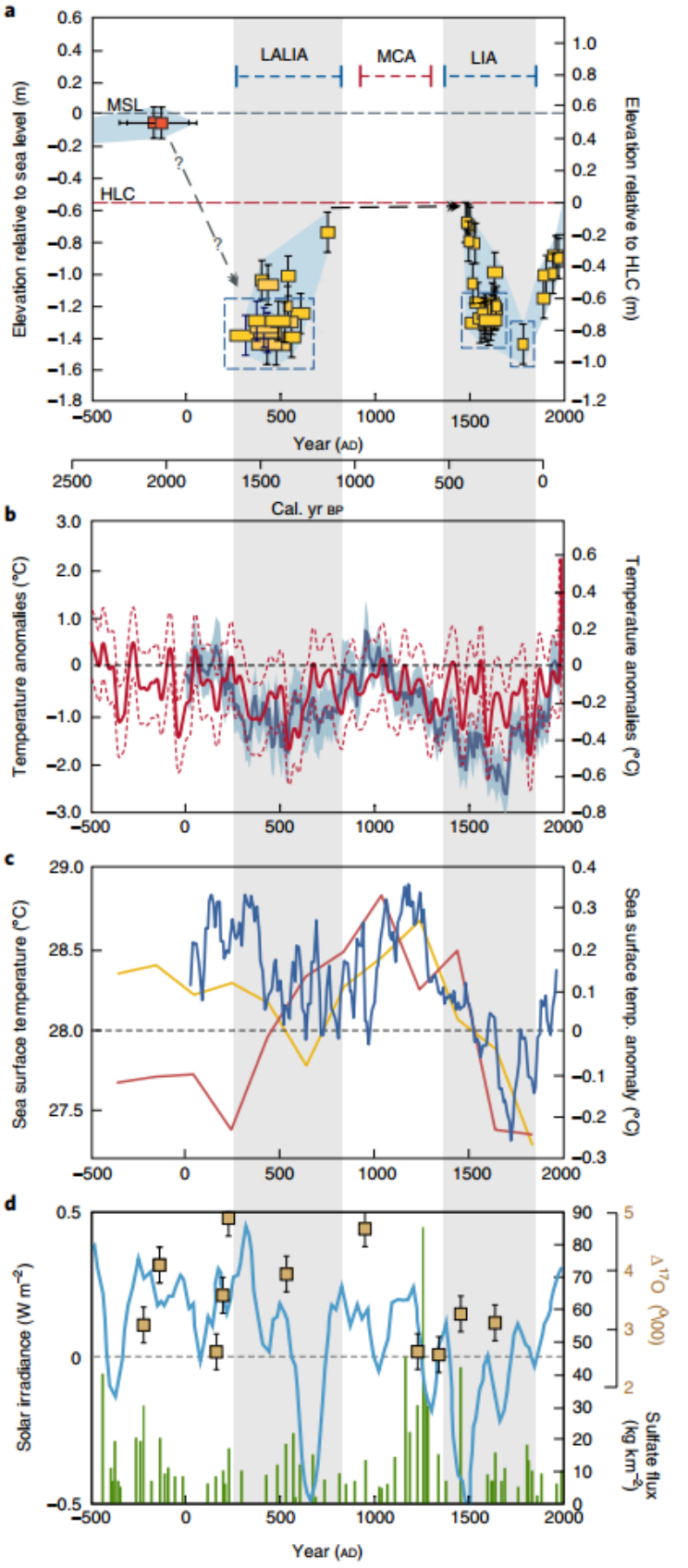

Figure 2. Reconstructed sea level in the central Indian Ocean and global paleoclimate variability over the past 2,500 years. **a**, The elevation and age of fossil microatolls from Mahutigalaa reef platform, Maldives.

Red boxes are two fossil microatolls from Funadhoo reef (central Maldives, Fig. 1a) that mark the end of the mid-late Holocene highstand and were dated using AMS; orange boxes are microatolls dated using U–Th method in this study (Supplementary Table 1), vertical error bars ±0.14 m. Age error bars are smaller than the size of symbols and the width of the boxes reflects the microatoll diameter. Dashed boxes indicate corals included in lowstand calculations. **b**, Reconstructed northern hemisphere (European) June, July and August temperature anomalies (red line and left y axis) relative to the 1901–2000 period (grey dashed line), the error is ±1 root mean square error (red dashed lines); and northern hemisphere decadal temperature variations (blue line, right y axis) with 2δ error (blue shading). **c**, A 2,000-year sea surface temperature reconstruction in Makassar Strait, Indonesia (blue line); SST reconstruction, for the West Pacific Warm Pool (red line) and southern Makassar Strait (orange line). **d**, Total solar irradiance (blue line), occurrence of major volcanic events through the Holocene (green bars) and volcanic events making major contributions to stratospheric sulfate levels based on $\Delta^{17}O$ analyses (brown squares), error bars are 1 s.d. The vertical grey shading denotes time periods of lower sea levels in the Mahutigalaa coral record and climatic cool periods. LIA, Little Ice Age; MCA, medieval climate anomaly; LALIA, Late Antiquity Little Ice Age.

4. IODP 的 1256D 孔完整的洋壳段面的磁性矿物学特征

翻译人：李园洁 liyj3@sustech.edu.cn

Krása D, Herrero-Bervera E, Acton G, et al. ***Magnetic mineralogy of a complete oceanic crustal section (IODP hole 1256D)*** *[M]//**The Earth's Magnetic Interior**. Springer, Dordrecht, 2011: 169-179.*

摘要：洋壳是海洋磁异常的载体因此是重要的地磁场信息记录体。ODP/IODP 的 1256D 孔第一次钻到完整的从洋壳到辉长岩序列的样品。我们利用扫描电子显微镜、微量分析和岩石磁性测量研究剩磁载体垂向上的变化。喷出层包含有枝状低温氧化钛磁铁矿(TMs)，比如原始组分与之前报道的大洋中脊玄武岩的值接近的钛磁赤铁矿。在整个喷出层，低温氧化（磁化）程度相当稳定。我们将观察到的居里温度随深度增加解释为钛磁赤铁矿向钛磁铁矿和非磁性相共生的亚微米转化，其中钛磁铁矿的 Ti 含量随着深度降低。下层席状岩墙，TMs 也是主要的磁性矿物。由于冷却速度较慢，它们大多数情况下被氧溶解成贫钛 TMs 和钛铁矿的薄片状共生体。磁矿物的蚀变程度比喷出层的更高。在辉长岩部分，TMs 的尺寸达到几十毫米，尽管由于出溶层的亚晶化，磁性颗粒大小保持在假单畴的范围。喷出层的热剩磁（TRM），保留主要的古地磁方向但是剩磁强度低。席状岩墙保留着热化学剩磁（TCRM）或热液蚀变过程的二次 TRM，而底部的辉长岩由于冷却速度慢在侵位后获得 TCRM。

ABSTRACT：Oceanic crust is the carrier of the marine magnetic anomalies and is therefore a valuable archive of geomagnetic information. ODP/IODP Hole 1256D was the first to sample an entire sequence of oceanic crust down to the gabbro. We studied the vertical variation of magnetic remanence carriers by means of scanning electron microscopy, microanalysis and rock magnetic measurements. The extrusive layer contains dendritic, low-temperature oxidized titanomagnetites (TMs), i.e. titanomaghemite, with initial compositions close to values previously reported for mid-ocean ridge basalts (MORB). The degree of low-temperature oxidation (maghemitisation) remains fairly constant across the extrusives. We explain the observed increase in Curie temperature with depth by submicron inversion of titanomaghemite to intergrowths of titanomagnetite and nonmagnetic phases, where the Ti-content of titanomagnetite is decreasing with depth. In the underlying sheeted dikes, TMs are again the primary magnetic mineral. Due to slower cooling, they

are in most cases oxy-exsolved into lamellar intergrowths of Ti-poor TMs and ilmenite. The magnetominerals are altered to a much higher degree than in the extrusives. In the gabbroic part of the section, TMs reach sizes up to several mm, although the magnetic grain size remains consistently in the pseudo-single-domain range because of grain subdivision by exsolution lamellae. The extrusives carry a thermoremanent magnetisation (TRM), retaining the primary paleomagnetic direction but with a reduced remanence intensity. The sheeted dikes hold a thermo-chemical remanent magnetization (TCRM) or secondary TRM acquired during hydrothermal alteration, whereas the underlying gabbro acquired a TCRM significantly after emplacement due to slow cooling at this depth.

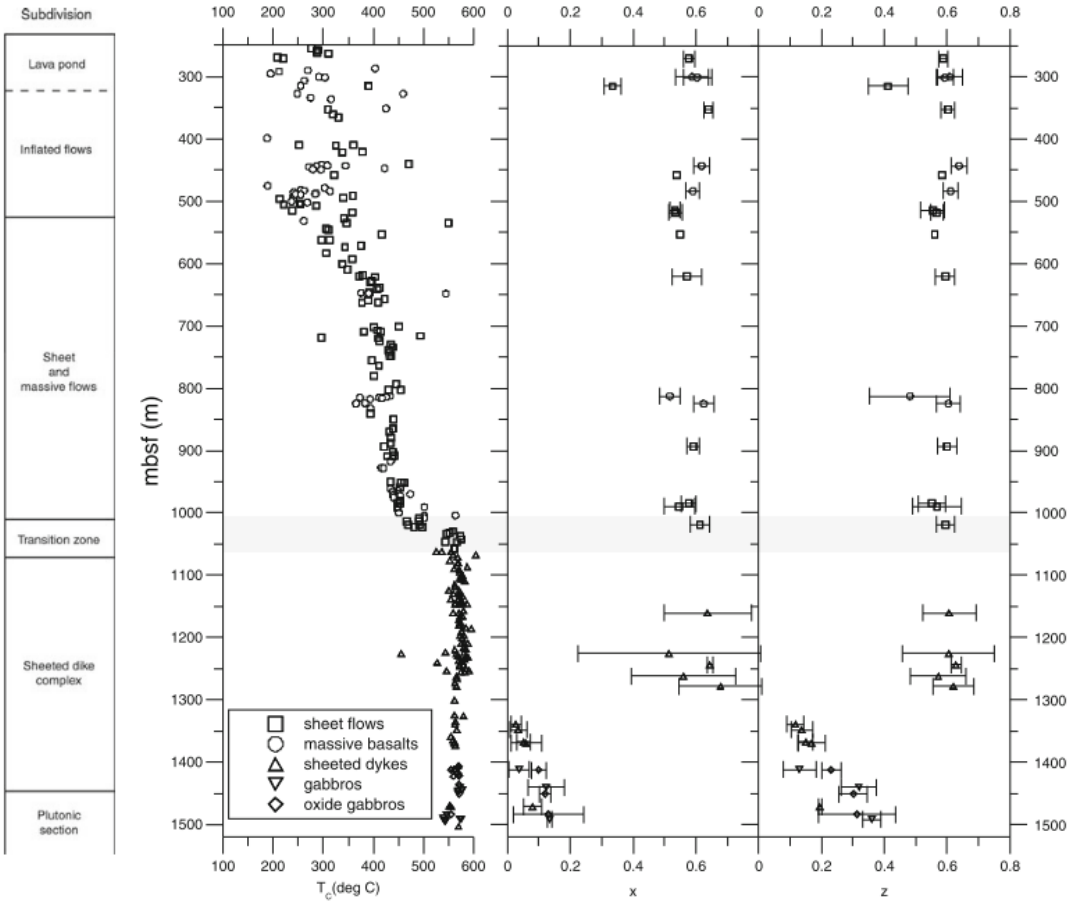

Figure 1. Downcore plots of TC, composition parameter x and oxidation parameter z vs. depth of the titanomagnetite fraction. The error bars for x and z show ± one standard deviation. In cases where they are missing, the analysis is based on only one particle measured. The shaded zone marks the transition from extrusives to intrusives (see simplified lithological column on the left-hand side)

5. 亚马逊低地在过去 45000 年中的水文气候变化

翻译人：杨会会 11849590@mail.sustech.edu.cn

*Wang X F, R L Edwards, A S Auler, et al.**Hydroclimate changes across the Amazon lowlands over the past 45,000 years** [J]. **Nature,** 2017, 541: 204-207.*

摘要：重建热带水文气候的历史是困难的，特别是对亚马逊盆地——地球上主要的深层大气对流中心之一。亚马逊盆地在冰期时变得非常干燥还是保持湿润一直以来都有争议，主要是因为大多数研究地点都位于盆地的边缘，也因为沉积物的保存、年代学的不确定性和地形环境会使解释变得复杂。本文表明，盆地中的降雨与冰期边界条件——温度和大气二氧化碳浓度的变化密切相关。我们对亚马逊东部的 Paraiso 洞穴石笋进行铀钍定年，建立了过去 45000 年，具有十几年分辨率的石笋氧同位素记录。我们将该氧同位素记录解译为降雨量记录。与现今降雨量水平对比，该地区在末次盛冰期的降雨量是今天的 58 %（大约 21000 年之前），在中全新世的降雨量是今天的 142 %（大约 6000 年之前）。我们发现，与来自亚马逊低地西部边缘的洞穴记录相比，在末次冰期亚马逊地区普遍较为干燥，循环水要少得多，植物的蒸腾作用可能也少得多，尽管雨林在这段时间内一直存在。

ABSTRACT: Reconstructing the history of tropical hydroclimates has been difficult, particularly for the Amazon basin—one of Earth's major centers of deep atmospheric convection1,2. For example, whether the Amazon basin was substantially drier3,4 or remained wet1,5 during glacial times has been controversial, largely because most study sites have been located on the periphery of the basin, and because interpretations can be complicated by sediment preservation, uncertainties in chronology, and topographical setting6. Here we show that rainfall in the basin responds closely to changes in glacial boundary conditions in terms of temperature and atmospheric concentrations of carbon dioxide7. Our results are based on a decadally resolved, uranium/thorium-dated, oxygen isotopic record for much of the past 45,000 years, obtained using speleothems from Paraíso Cave in eastern Amazonia; we interpret the record as being broadly related to precipitation. Relative to modern levels, precipitation in the region was about 58% during the Last Glacial Maximum (around 21,000 years ago) and 142% during the mid-Holocene epoch (about 6,000 years ago). We find that, as compared with cave records from the western edge of the lowlands, the Amazon was widely drier

during the last glacial period, with much less recycling of water and probably reduced plant transpiration, although the rainforest persisted throughout this time.

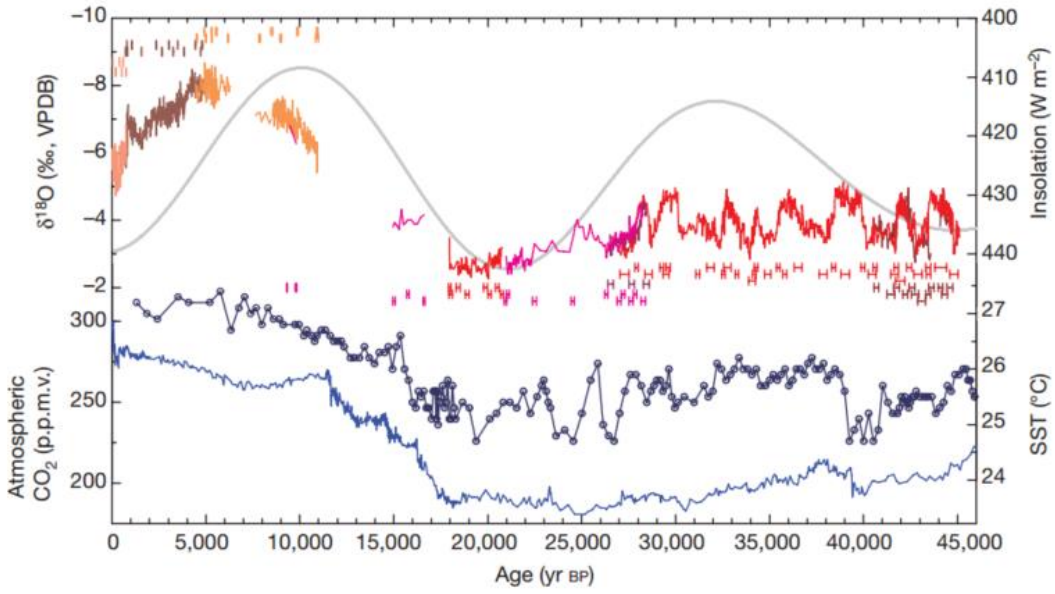

Figure 1. Paraíso speleothem record, and comparisons with local summer insolation, tropical Atlantic SST and atmospheric CO2 concentration. Top, the Paraíso record is spliced by replicated δ18O profiles from seven stalagmite samples. Uranium/thorium dates and error bars (2σ) are shown, with different colors for each stalagmite sample. The record covers the past 45,000 years, with three short gaps: ~16.6 kyr to 18.0 kyr bp, ~10.9 kyr to 15.0 kyr bp, and ~6.3 kyr to 7.6 kyr bp. The insolation at 5° S in January is also shown, in grey; note that the insolation is plotted in a reversed scale, as proposed in ref. 16. The correlation between the Paraíso δ18O values and local insolation is, however, not strong. See Extended Data Fig. 6 for more details. Centre, tropical Atlantic alkenone SST reconstruction from sediment core GeoB 3910-2 (in dark blue, ref. 19). Bottom, changes in atmospheric CO2 concentration7 (in light blue; see also Extended Data Fig. 7). p.p.m.v., parts per million by volume.

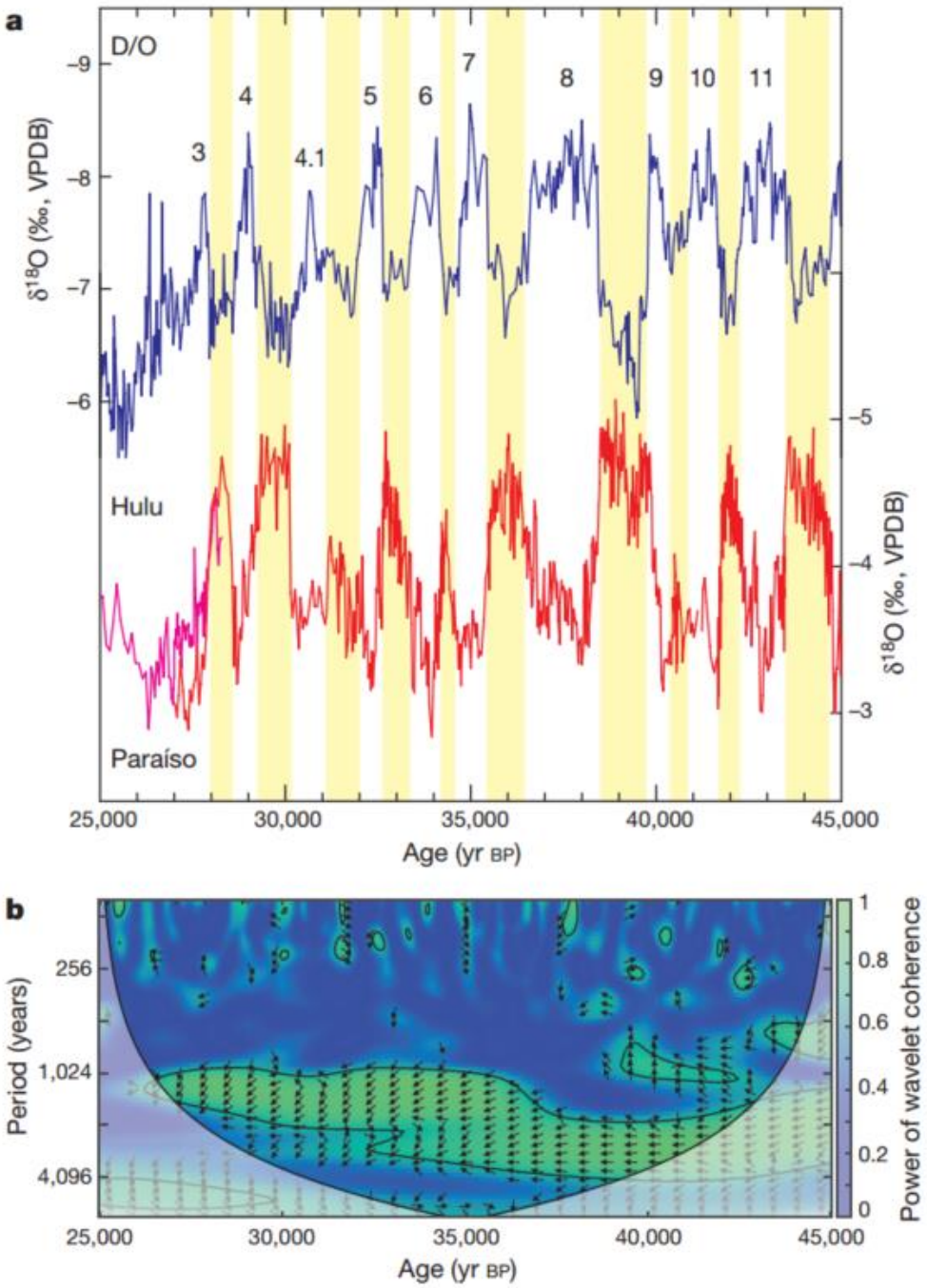

Figure 2. Comparisons of eastern Amazon and eastern China stalagmite records. **a**, Stalagmite $\delta^{18}O$ records from the eastern Amazon (Paraíso, in red and pink) and eastern China (Hulu, in blue)[24] for the time interval from 25 kyr bp to 45 kyr bp. These records are oppositely correlated on millennial timescales, suggesting an anti-phased relationship for rainfall between the two regions. D/O climate events (numbered from 3 to 11) are also marked. **b**, The strong anti-phased correlation between the two records on millennial timescales is confirmed by squared wavelet coherence (http://noc.ac.uk/using science/crosswavelet-waveletcoherence) of the two standardized time series. The 5% significance level against red noise is shown as a thick contour. The relative phase relationship between the two time series is shown as arrows, with antiphase pointing left.

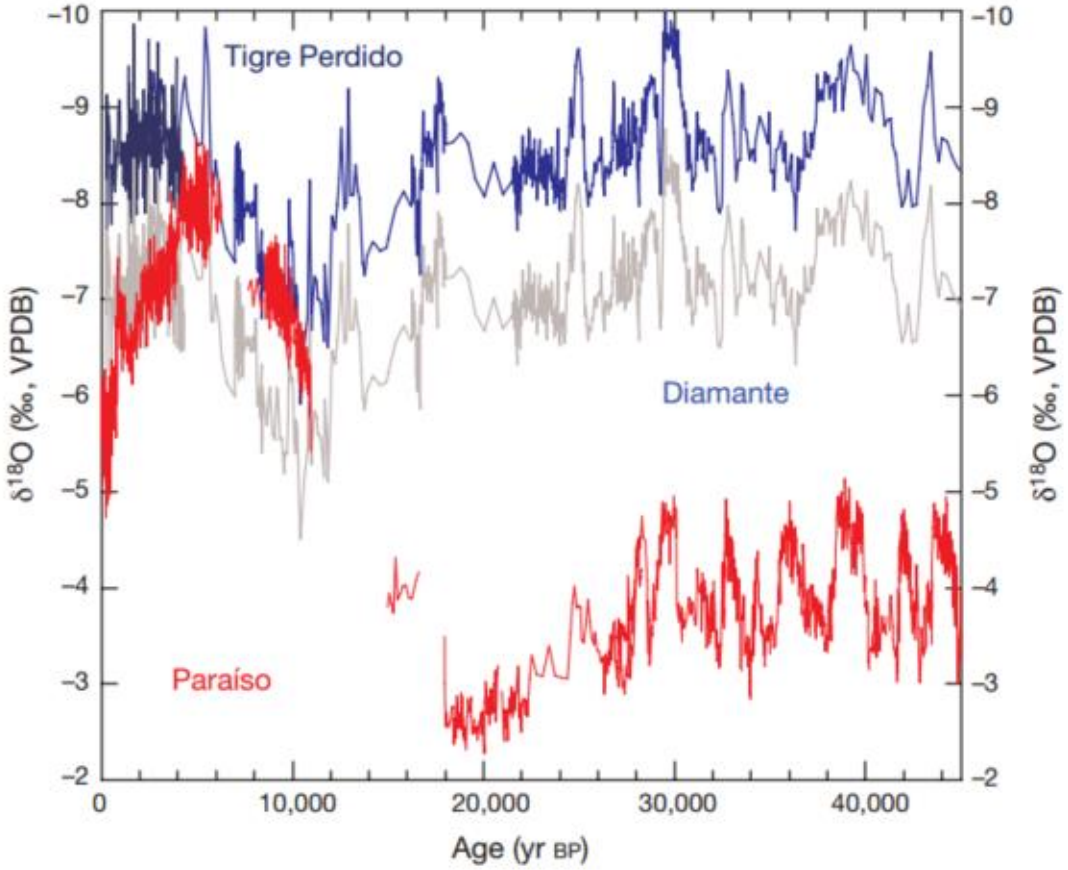

Figure 3. Comparisons of speleothem records from the eastern and western Amazon. The eastern Amazon $\delta^{18}O$ record (red) is from Paraíso cave; the speleothem $\delta^{18}O$ records in the western Amazon are from Diamante[17] (blue) and Tigre Perdido[9] (dark blue; left) caves. All three records are absolutely dated with uranium/thorium dating techniques. The original records from the western Amazon are shown in grey; they were then shifted 1.4‰ negatively to account for the oxygen isotopic fractionation that resulted from a difference in cave temperature between the western sites and Paraíso cave in the east (see Methods).

6. 晚全新世以来跨越喜马拉雅干旱地区的陆地衰退：人类影响和干旱化

翻译人：王浩森 502691781@qq.com

Menges J, Hovius N, Andermann C, et al. ***Late Holocene landscape collapse of a Trans-Himalayan dryland: Human impact and aridification****[J].* ***Geophysical Research Letters****, 2019.*

摘要：土壤退化是对全球生态系统变的日益严重的威胁。土壤流失通常是非线性的，一旦达到临界点，就会从稳定的生态地貌状态迅速恶化。 虽然在样本土地规模上研究了土壤流失阈值，但是对于实际土地而言，对临界点的必要条件和充分条件的定量限制很少。本文记录了青藏高原边缘的整个土地的生态地貌转折点，并量化了其驱动因素和侵蚀结果。结果表明，在全新世的大部分时间里，在尼泊尔的上卡利甘达基山谷上游，土壤在潮湿条件下普遍形成。同时数据表明，经过一段时间的人为影响和植被覆盖度下降之后，相对湿度和降水量在 200 mm /年以下降低 20％，在 1.6 ka 之后阻止了土壤形成，并促进了广泛的沟壑和快速的土壤流失，对生态系统服务产生了不可逆转的后果。

ABSTRACT: Soil degradation is a severe and growing threat to ecosystem services globally. Soil loss is often nonlinear, involving a rapid deterioration from a stable eco-geomorphic state once a tipping point is reached. Soil loss thresholds have been studied at plot scale, but for landscapes, quantitative constraints on the necessary and sufficient conditions for tipping points are rare. Here, we document a landscape-wide eco-geomorphic tipping point at the edge of the Tibetan Plateau and quantify its drivers and erosional consequences. We show that in the upper Kali Gandaki valley, Nepal, soil formation prevailed under wetter conditions during much of the Holocene. Our data suggest that after a period of human pressure and declining vegetation cover, a 20% reduction of relative humidity and precipitation below 200 mm/year halted soil formation after 1.6 ka and promoted widespread gullying and rapid soil loss, with irreversible consequences for ecosystem services.

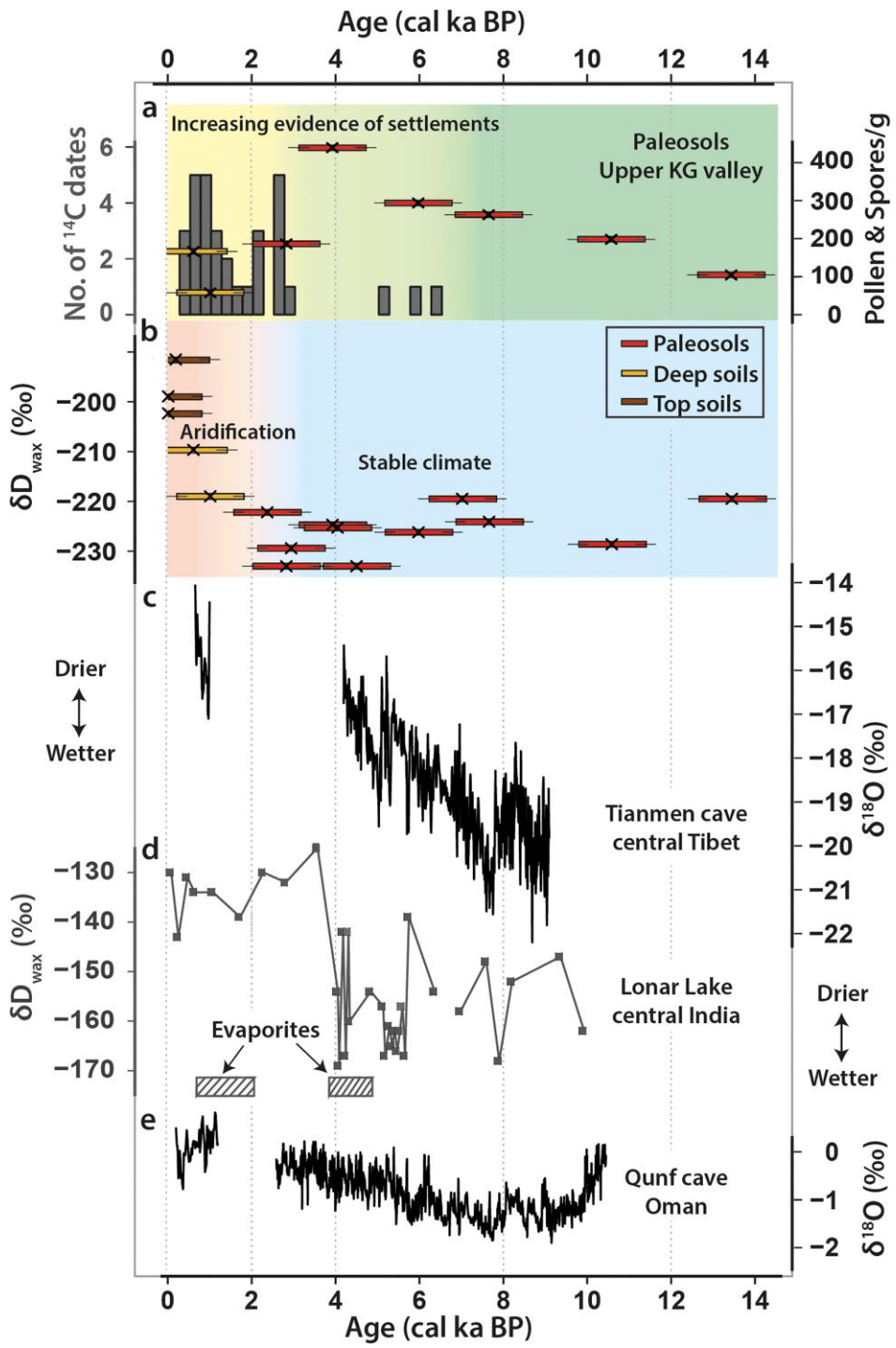

Figure 1. Paleosol data from the upper KG valley and Holocene climate records from the wider ISM region. (a) Histogram of ^{14}C-dated archeological and charcoal samples (gray) in the upper KG valley (Saijo & Tanaka, 2002; Simons et al., 1994) and this study (left *y* axis) and humin fraction ^{14}C ages (*x*) with integration time of 1.6 ± 0.5 Kyr versus summed pollen and spores concentrations for paleosols (red) and deep soils (yellow) (right *y* axis). (b) Humin fraction 14C ages (*x*) with integration time of 1.6 ± 0.5 Kyr versus δD for paleosols (red), deep soils (yellow), and modern topsoils (brown). (c) $\delta^{18}O$ speleothem record from Tianmen cave, central Tibet (Cai et al., 2012). (d) δDwax values and occurrence of Galussite crystals in Lonar Lake, Central India (Prasad et al., 2014; Sarkar et al., 2015). (e) $\delta^{18}O$ speleothem record from Qunf cave, Oman (Fleitmann et al., 2003).

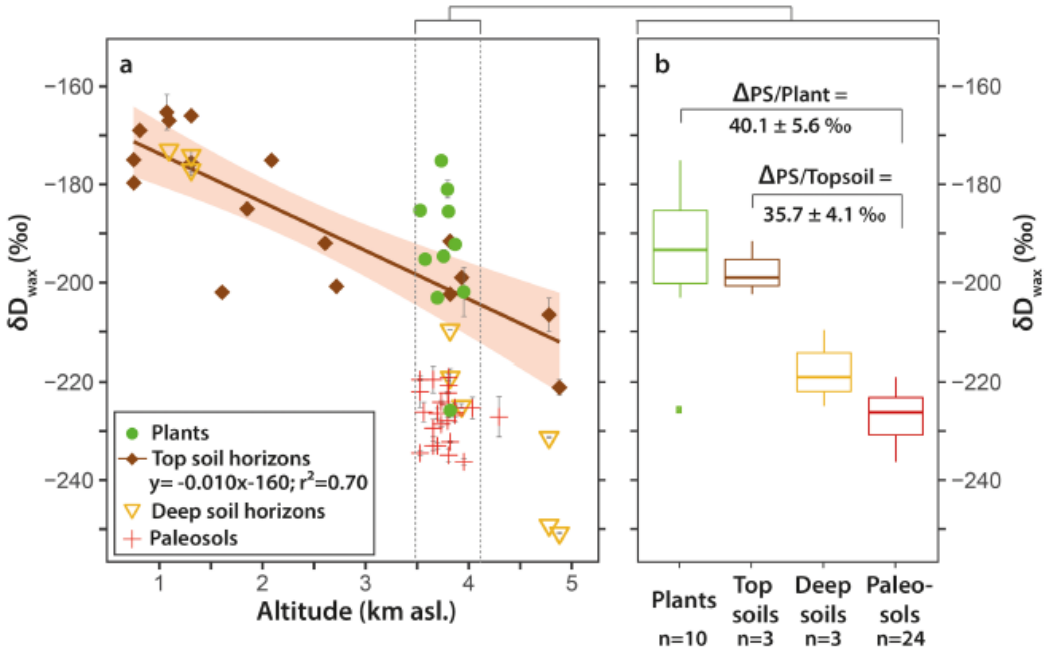

Figure 2. (a) δD_{wax} values for *n*-C_{29} from modern plants (*Caragana gerardiana*) and topsoils, deeper soils, and paleosols plotted against sampling altitude; confidence interval around regression at 95%. (b) Box and whisker plots showing distribution of δD_{wax} values among different sample types from 3,500 to 4,200 m asl. $\Delta_{PS/Plant}$ denotes offset between paleosols and *Caragana gerardiana* and $\Delta_{PS/Topsoil}$ between paleosols and active topsoils. Boxes extend to first and third quartile and whiskers to extreme values within 1.5 interquartile range.

7. 北大西洋深海平原沉积物早期成岩作用：以岩石磁学和地球化学指标为特征

翻译人：王敦繁 dunfan-w@foxmail.com

Robinson S G, Sahota J T S, Oldfield F. ***Early diagenesis in North Atlantic abyssal plain sediments characterized by rock-magnetic and geochemical indices****[J].* ***Marine Geology,*** *2000, 163(1-4):77-107.*

摘要：本文研究了位于非洲大陆西北边缘以西马德拉深海平原晚第四纪浊积层序的早期成岩作用。在该地区的 3 个沉积物岩心中，固相地球化学氧化还原敏感性离子指数与岩石磁性参数进行了比较，作为成岩作用表征的代用指标。以泥质为主的远端浊积岩的侵位主要是由于海平面的冰川升降变化造成的，它们来自非洲西北部边缘的不同地点，也来自加那利群岛的侧翼。因此，浊积岩的组成是变化的，特别是在碳酸盐、碎屑磁性矿物和有机碳含量方面。在富有机质(0.5% Corg)浊积岩层内，有机碎屑再矿化分两个阶段进行。初期涉及到次元还原。成岩作用发生在孔隙水 O_2 耗尽之后，而后期则发生氧化成岩作用，由于上覆海水中 O_2 的扩散，氧化锋通过沉积物缓慢下降。这些沉积物的岩石-磁性参数，如果在无碳酸盐的基础上表达，则显示出的碎屑铁磁性铁的显著消耗。在亚成岩过程中，富有机质浊积岩中出现了氧化物颗粒。磁性参数的归一化商和所选样品的剩磁-矫顽力剖面也表明还原性成岩作用是一个铁磁性晶粒尺寸选择过程，但对倾斜的反铁磁影响很小。沉积物中的氧化物。因此，当铁磁性颗粒逐渐溶解时，这些成分在磁性组合中变得相对丰富。然而，在所有三个研究的岩心中，都有明确的证据表明，在富含有机浊积岩的深处，在活性和化石氧化之下存在超细铁磁性氧化铁颗粒。这些颗粒可能与活的趋磁细菌群有关，它们栖息在有机丰富的层位上，通常与成岩作用有关的细菌介导的反应形成。这些结果与前人在半远洋沉积物中成岩作用的研究结果相一致，阐明了涉及深海沉积物中铁相转变的成岩作用的氧化还原过程。

ABSTRACT： Processes of early diagenesis are investigated in a sequence of late Quaternary turbiditic sediments from the Madeira Abyssal Plain MAP., west of the NW African continental margin. In three sediment cores from this region, solid-phase geochemical indices of redox-sensitive ion mobilization are compared with rock-magnetic parameters as proxies for diagenesis characterization. The mud-dominated, distal turbidites are emplaced mainly as a result of glacio-eustatic changes in sea-level, and derive both from different sites on the NW African margin, and

from the flanks of the Canary Islands. Thus, the turbidites are of variable composition, especially in terms of carbonate, detrital magnetic mineral, and organic carbon content. Within organic-rich (0.5% Corg) turbidite horizons, remineralization of organic detritus proceeds in two stages. The initial stage involves suboxic reductive. diagenesis, following depletion of pore-water O_2, while the later stage involves oxidative diagenesis associated with the slow descent of an oxidation front through the sediment, due to diffusion of O_2 from the overlying seawater. Rock-magnetic parameters of these sediments, when expressed on a carbonate-free basis, reveal that significant depletion of detrital ferrimagnetic iron Fe^{+2}/Fe^{+3}. oxide grains have occurred within the organic-rich turbidites during suboxic diagenesis. Normalized quotients of magnetic parameters, and remanence-coercivity profiles of selected samples, also show that reductive diagenesis is a ferrimagnetic grain size-selective process, but it has a minimal effect on the canted-antiferromagnetic Fe^{+3}. oxides in the sediment. Such components, if present, therefore become relatively enriched in magnetic assemblages as the ferrimagnetic grains are progressively dissolved. In all three cores studied, however, there is clear evidence for the presence of ultrafine ferrimagnetic iron oxide grains at depth within the suboxic zones of organic-rich turbidites, beneath both active and fossil oxidation fronts. These grains are probably associated with populations of live magnetotactic bacteria which inhabit such organic-rich horizons, and which form a link in the chain of bacterially mediated reactions normally associated with suboxic diagenesis. These results comply with previous observations made in studies of suboxic diagenesis in hemipelagic sediments, and demonstrate the value of rapid and non-destructive rock-magnetic measurements for illuminating redoxomorphic processes of diagenesis involving transformation of iron phases in deep-sea sediments.

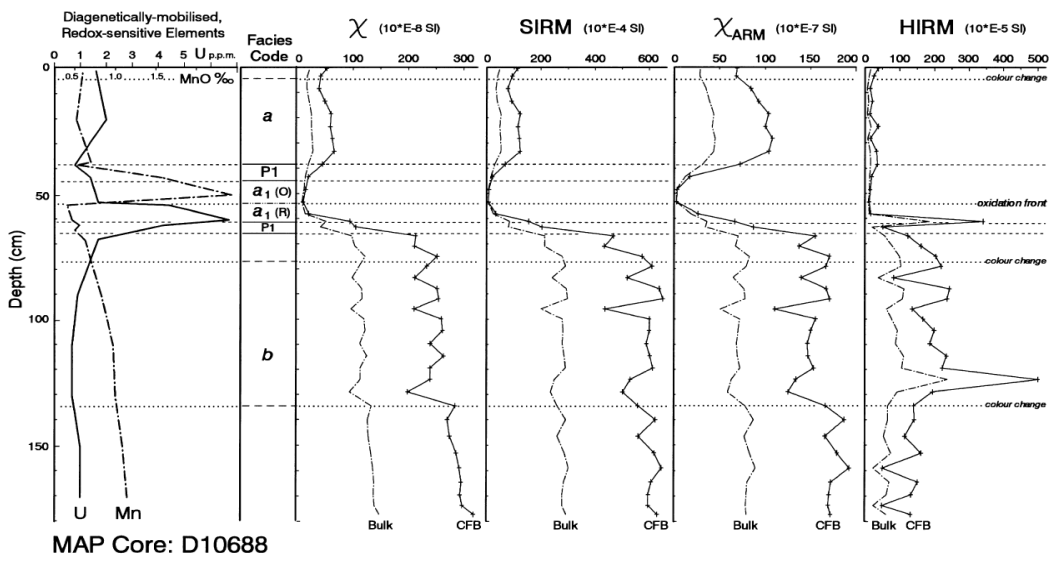

Figure 1. Concentration-dependent rock magnetic parameters of MAP core D10688, 0–180 cm, compared with geochemical indices of redoxomorphic diagenesis in the sediment. Magnetic parameters are expressed both on a bulk-sediment (Bulk). and a carbonate-free basis (CFB).

8. Ori 地块磁异常图及其对大洋高原形成的意义

翻译人：曹伟 11930854@mail.sustech.edu.cn

Huang Y, Sager W W, Tominaga M, et al. ***Magnetic anomaly map of Ori Massif and its implications for oceanic plateau formation****[J].* ***Earth and Planetary Science Letters****, 2018, 501: 46-55.*

摘要：许多海底高原位于洋中脊或洋中脊附近。为了解释高原体积和厚度与正常洋壳的差异，通常假设热点-脊相互作用，但这种相互作用的机理仍不清楚。Shatsky 海隆是一座大型火山构成的三联点，形成于晚侏罗世至早白垩世。最近的钻探和地震调查表明，Ori 地块的中部构造是一座中央火山。自相矛盾的是，追踪的条带状磁异常横跨了部分 Ori 地块，这意味着该处在形成了洋中脊。在这项研究中，我们研究了 Ori 地块及其周围的磁异常，以获得有关这座海底火山高原形成的深入了解。我们对 21 艘船测磁异常数据进行校正、合并和网格化，形成磁异常图，并通过正反磁模拟研究了 Ori 地块的磁性结构。结果表明，这座大型火山高原的主要异常特征是正、反极性磁化块体交替产生的线性磁异常，类似于扩张脊记录的磁异常。这种异常特征不可能是由长时间流出的熔岩流所形成的中央火山，这意味着 Ori 火山喷发必须被限制在脊轴附近。Ori 地块南北边界的磁异常组合意味着它处于一个三联点处，表明在沙茨基隆起形成过程中存在复杂的洋脊构造。Ori 地块被线性磁异常横穿这个令人惊讶的发现表明，尽管洋壳厚度很大，海洋高原仍然可以记录海底扩展磁异常。此外，其他的海洋高原也记录了线性磁异常，这意味着不同板块边界与海洋高原火山存在着联系。

ABSTRACT： Many oceanic plateaus have been emplaced at or adjacent to mid-ocean ridges. To explain plateau volume and thickened crust compared to normal oceanic crust, hotspot–ridge interaction is commonly assumed, but the manner of interaction remains unclear. The Shatsky Rise oceanic plateau is a large volcanic mountain that formed at a triple junction during Late Jurassic and Early Cretaceous time. Recent drilling and seismic investigations suggest that the intermediate edifice in the rise, Ori Massif, is a central volcano. Paradoxically, magnetic lineations were traced across parts of Ori Massif, implying formation at a spreading ridge. In this study, we examined magnetic anomalies over and around Ori Massif to obtain insights about the formation of this volcanic edifice. Magnetic data from 21 cruises were corrected, combined, and gridded to construct a magnetic anomaly map. Forward and inverse magnetic modeling was done to investigate the

magnetic structure of Ori Massif. The results imply that this large volcanic edifice is predominantly characterized by linear magnetic anomalies resulting from alternating normal and reversed polarity magnetization blocks, analogous to magnetic anomalies recorded by spreading-ridges. This magnetic structure is not expected for a central volcano that was built by long runout lava flows, implying that Ori Massif eruptions must have been constrained near the ridge axis. Magnetic bights on the north and south boundaries of Ori Massif imply that it was bracketed by triple junctions, indicating complex ridge tectonics during the formation of Shatsky Rise. The surprising finding that Ori Massif is traversed by coherent linear magnetic anomalies indicates that oceanic plateaus can record seafloor spreading magnetic anomalies despite large crustal thickness. Other oceanic plateaus also record linear magnetic anomalies, implying a link between divergent plate boundaries and oceanic plateau volcanism.

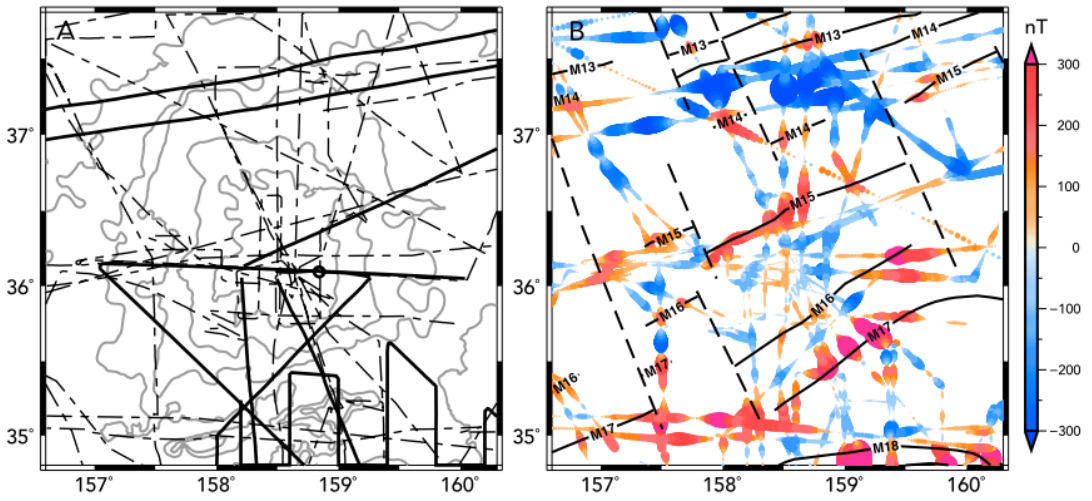

Figure 1. (A) Chart of data tracks used in this study. Dashed lines denote cruises used in Nakanishi et al. (1999); solid lines are newer data (Table 1). Gray contours show bathymetry at 500-m intervals. (B) Data coverage and anomalies. Data point size is based on anomaly amplitude (larger point = larger anomaly absolute value) and color denotes both amplitude and sign. Annotated solid lines denote magnetic isochrons and heavy dashed lines represent fracture zones (Nakanishi et al., 1999).

9. 南海北部河流沉积物的源-汇过程:来自华南沿海河流沉积物的约束

翻译人：刘伟 inewway@163.com

Cao L, Liu J, Shi X, et al. ***Source-to-sink processes of fluvial sediments in the northern South China Sea: Constraints from river sediments in the coastal region of South China****[J].* ***Journal of Asian Earth Sciences****, 2019, 185: 104020.*

摘要：对华南沿海 9 条河流的细粒沉积物组分(< 63μm)和 14 个南海北部大陆架表层沉积物进行主、微量元素和 Sr-Nd 同位素分析以区分沉积物源，确定控制南海北部大陆架地球化学组成的分布因素。结果表明，该地区沉积物的地球化学组成各不相同，可作为研究区沉积物物源识别的依据。这些河流沉积物主要沉积在南海北部大陆架的大陆架上，其影响在不同位置存在差异。珠江口东部和西部沉积物中的不同 εNd 和 $^{87}Sr/^{86}Sr$ 值，指示风化强度从东部到西部变化很大。南海陆架沉积物的主要来源为华南东部和西部沿海河流、台湾西部沿海河流和陆架残余沉积物。

ABSTRACT: The fine-grained fractions (<63 μm) of nine fluvial sediments from South China coastal rivers (SCCR) and fourteen surface sediments from the continental shelf of the northern South China Sea (NSCS) are analyzed to determine the major and trace elements and Sr-Nd isotope compositions and differentiate the sediment sources and factors that control the distribution of geochemical compositions on the NSCS shelf. The results reveal that the geochemical compositions of sediments from the SCCR differ from each other and can be utilized to identify the sediment provenance in the study area. These river sediments are mostly deposited on the continental shelf of the NSCS, and their influence is different in various locations. Sediments on the eastern and western sides of the Pearl River mouth have different εNd values and $^{87}Sr/^{86}Sr$ ratios, indicating that the weathering intensity varies greatly from the eastern side to the western side. The main sediment sources in the NSCS shelf contain fluvial sediments discharged by the eastern and western coastal rivers of South China and the coastal rivers of western Taiwan and relict sediments on the continental shelf.

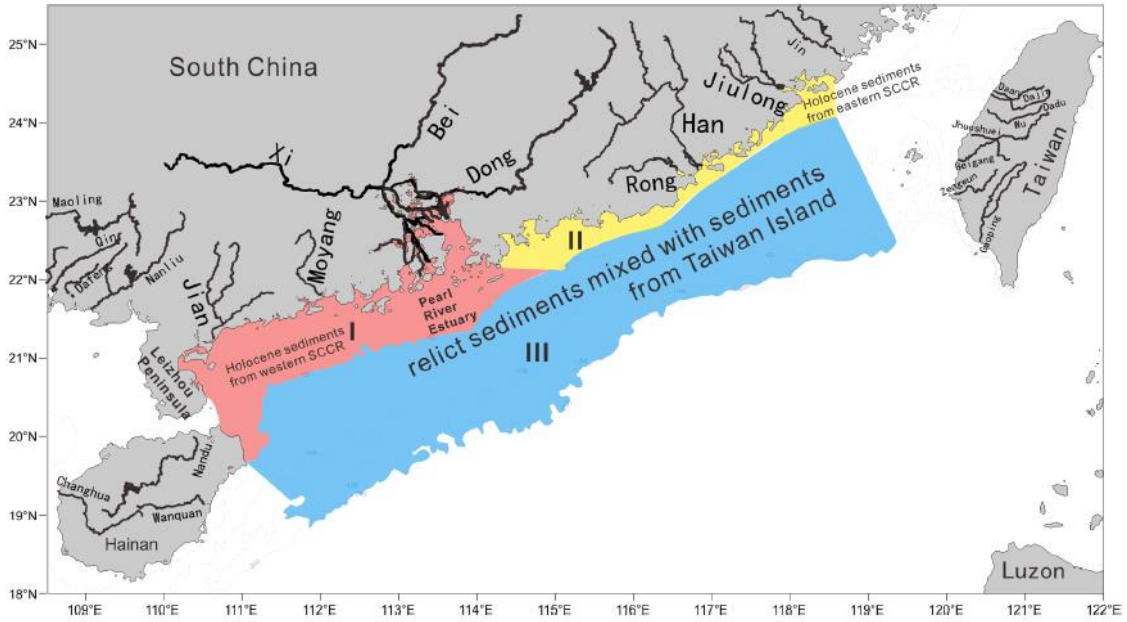

Figure 1. Depositional patterns in the NSCS shelf. The NSCS shelf can be divided into three depositional areas. Areas (indicating a strong chemical weather degree with high CIA values ranging from 77 to 82) and II (presenting low εNd values ranging from 10.53 to 11.16, which are influenced by sediments from the east South China coast) are dominated by Holocene sediments from the western and eastern SCCR, respectively, while Area III (indicating a weak chemical weathering degree with low CIA values varying from 68 to 76) is dominated by relict sediments mixed with sediments from Taiwan Island.

10. 三氧同位素在石笋研究中的应用

翻译人：郑威 11930589@mail.sustech.edu.cn

Sha L, Mahata S, Duan P, et al. ***A novel application of triple oxygen isotope ratios of speleothems****[J].* ***Geochimica et Cosmochimica Acta****, 2019.*

摘要：本文通过O_2-CO_2 Pt 催化氧同位素平衡获得了三氧同位素的数据。新的高精度的石笋$\Delta^{17}O$数据足以解读微弱的水文气候讯号。此外，我们通过在17±1℃的温度下收集的两组现代碳酸盐-滴水成对样品确定了三氧同位素的分馏参数，这是从石笋代用指标数据中计算在洞穴位置的母大气水的三氧同位素组分的前提条件。基于这个标准，我们使用三个地区的石笋代用指标数据反演了具有明显气候转化特征的母水的三氧同位素组分。所得的氧同位素数据与全球大气降水线（GMWL）密切相关，为该方法提供了初步的验证。石笋$\Delta^{17}O$数据表明，中亚地区深海氧同位素阶段5d和5e期间的差异为21/meg，而地中海东部地区中全新世和末次冰盛期之间的差异为15/meg，这展现了水汽源的变化和（或）分馏历史记录。出乎意料的是，南美（亚马逊西部）和亚洲（中国南部）的季风区的冰期、间冰期的样品并没有可测量的$\Delta^{17}O$差异，这意味着至少在相对湿度上，有稳定的水汽源贯穿整个冰期间冰期循环。值得注意的是，亚马逊西部样品的$\Delta^{17}O$的值（~20/meg）显著高于亚洲季风区的样品，这表明在中全新世到末次盛冰期期间，西亚马逊水汽源轨迹的相对湿度较低。同样，地中海东部地区$\Delta^{17}O$的值（19-55/meg）显著高于中亚地区同时期的样品，指示即使在相同的西风环流区域也有不同的水文环境或水汽源。因此，石笋$\Delta^{17}O$数据可能为理解区域和全球水文气候动力提供新的重要约束。

ABSTRACT： We present triple oxygen isotope data from speleothems obtained by an O_2-CO_2 Pt-catalyzed oxygen-isotope equilibration method. The high precision (9 per meg or better, 1σ SD) of our new speleothem $\Delta^{17}O$ (carbonate ^{17}O anomaly) data is sufficient to resolve subtle hydroclimatic signals. In addition, we determined triple oxygen isotope fractionation factors through two sets of modern paired carbonate-dripwater samples collected at a temperature of 17 ±1°C, which is prerequisite to the calculation of triple oxygen isotope compositions of parent meteoric waters at cave sites from speleothem proxy data. Based on this calibration, we back calculated triple oxygen isotope compositions of parent waters across well-characterized climate transitions using

speleothem proxy data from three regions. Resulting oxygen-isotope data closely track the Global Meteoric Water Line (GMWL), providing a preliminary validation of the method. Our speleothem $\Delta^{17}O$ data indicate a 21 per meg difference between Marine Isotope Stage 5d and 5e in samples from Central Asia and a 15 per meg difference between the Middle Holocene and Last Glacial Maximum in samples from the eastern Mediterranean, suggesting a shift in moisture source and/or fractionation history. Unexpectedly, there were no measurable $\Delta^{17}O$ differences between glacial and interglacial samples from both the South American (western Amazon) and Asian (southern China) monsoon domains, implying consistent moisture-source conditions across glacial and interglacial cycles, at least in terms of relative humidity. Remarkably, $\Delta^{17}O$ values from the western Amazonian samples are significantly higher (~20 per meg) than those from Asian monsoon regions, suggesting lower relative humidity along moisture trajectories in the western Amazon during the Middle Holocene and Last Glacial period. Similarly, $\Delta^{17}O$ values of the eastern Mediterranean samples are significantly higher (19–55 per meg) than those of coeval samples from Central Asia, implying different hydrological environments or moisture sources despite being in the same westerly circulation domain. Speleothem $\Delta^{17}O$ data may thus provide new and important constraints for understanding regional and global hydroclimate dynamics.

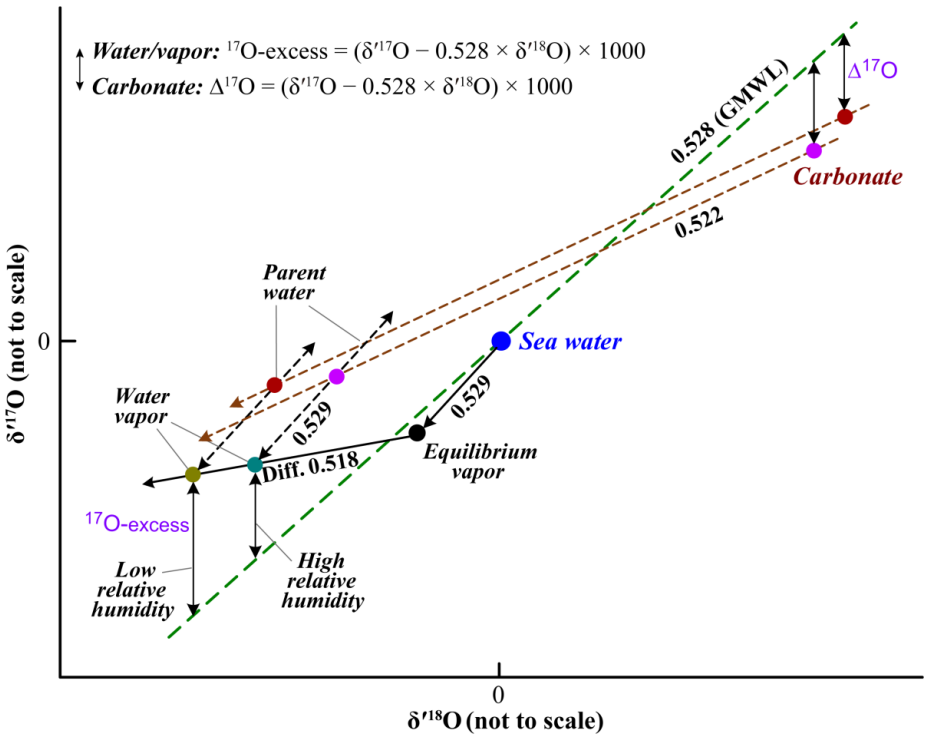

Figure 1. Schematic presentation of $\delta^{17}O$-$\delta^{18}O$-$\Delta^{17}O$ (carbonates)/^{17}O-excess (water) systematics during carbonate deposition (dashed brown lines show a slope of 0.522; this study), vapor evaporation (0.529,

Luz and Barkan, 2010), diffusion (0.518, Luz and Barkan, 2010), and condensation (0.529, Luz and Barkan, 2010) processes (see text for detailed explanations). Dashed green line indicates the Global Meteoric Water Line (GMWL) (0.528, Meijer and Li, 1998, Landais et al., 2008, Luz and Barkan, 2010). $\delta'^{17}O = 1000 \times \ln(1+\delta^{17}O/1000)$ and $\delta'^{18}O = 1000 \times \ln(1+\delta^{18}O/1000)$.